American Mineralogist, Volume 88, pages xxx–xxx, 2003

A technique for measuring 3D crystal-size distributions of prismatic microlites in obsidian

JONATHAN M. CASTRO,[1,*] KATHARINE V. CASHMAN,[2] AND MICHAEL MANGA[3]

[1]Oberlin College, Geology, 52 West Lorain St., Oberlin, Ohio 44074, U.S.A.
[2]University of Oregon, Geological Sciences, 1272 Geological Sciences, University of Oregon, Eugene, Oregon 97403, U.S.A.
[3]University of California Berkeley, Earth and Planetary Science, 173 McCone Hall, Berkeley, California 94720-4767, U.S.A.
{{Author Query: Please check addresses for all of the authors, pulled from web. In future papers, please include in text}}

ABSTRACT

We describe a technique for determining the 3D size, shape, and number density of prismatic microlites in obsidian. The procedure involves collecting a series of optical photomicrographs at successive levels in a transparent thin section with a petrographic microscope and digital camera. These images are combined to form 3D stacks with *NIH Image* software. The number, position, orientation, and projection length of each microlite in the stack are then determined, and these data are used to calculate the true length and number density. CSDs based on direct measurements exhibit asymptotic, lognormal, and near-lognormal profiles. These forms, in addition to broad variations in crystal aspect ratio suggest that microlites experienced a range of growth rates. Textural parameters (e.g., total crystal-number density and volume) determined from regressions of linear CSDs under the assumption of constant growth rate compare well with directly measured parameters.

We compared **{AU: word was missing – change OK?}** CSDs based on 3D measurements with those based on 2D measurements of intersection length and area number density. Stereological conversions of 2D data are necessary owing to the cut-section effect and intersection probability problem. We performed corrections with three widely used algorithms and, thus, our comparisons test the accuracy of **{AU: word was missing – change OK?}** these correction methods as applied to prismatic microlites in obsidian. CSDs based on 3D measurements are linear over most of the size range. In contrast, conversion programs produce kinked CSDs, with large positive errors in population density at small crystal size. Errors in population density are caused by shape (aspect ratio) variability in the sample population. Conversion programs, which assume a constant shape, overestimate the number of small crystals owing to a large number of intersections along the short crystal dimension. In the real population, these intersections correspond to a wide range of true lengths. Consequently, CSDs constructed from intersection lengths are kinked rather than linear. Kinked and curved CSDs have been interpreted to result from mixing of distinct crystal populations, sharp variations in growth and/or nucleation rate, or from crystal settling. Our results suggest that nonlinear CSDs in some cases may also arise as an artifact of shape variability in the natural population.

INTRODUCTION

Crystal-size distributions (CSDs) are widely used to interpret magmatic processes from the textures preserved in volcanic and plutonic rocks (Cashman and Marsh 1988; Waters and Boudreau 1996; Zieg and Marsh 2002). In igneous rocks, CSDs may provide information on the cooling history (Armienti et al. 1994; Cashman et al. 1999), crystal growth rates (e.g., Cashman 1992, 1993; Wilhelm and Worner 1996), and magmatic processes such as crystal settling and resorption (Marsh 1998). CSDs also have been used to infer magma chamber dynamics (Mangan 1990) and detailed eruptive histories (e.g., Higgins 1996; Hammer et al. 1999). At the core of CSD analysis is a semi-logarithmic plot of the population density (n)—the number of crystals of a given size per unit volume, vs. size (commonly apparent crystal length; Randolf and Larson 1971). Textural parameters, such as the dominant crystal size, crystal number density, and crystal volume fraction, can be derived from regressions of linear CSDs (e.g., Marsh 1988; Cashman 1990), however, interpreting magmatic processes from CSDs may not be so straightforward (e.g., Pan 2001, 2002; Eberl et al. 2002; Higgins 2002a, 2002b; Marsh and Higgins 2002; Schaeben et al. 2002).

The accuracy of CSD-derived textural parameters depends largely on the manner in which CSDs are constructed, and on the extent to which the crystal population conforms to a CSD model (e.g., Marsh 1988; Eberl et al. 2002). Direct 3D measurements of crystal size provide the most accurate description of the population (e.g., Armienti et al. 1994; Dunbar et al. 1994; Bindeman 2003). However, because of the time and difficulty associated with making accurate measurements in 3D, most published CSDs of igneous rocks are based on 2D measurements of crystal intersection size and area number density. Conversion of 2D data to 3D requires a number of stereological corrections to account for: (1) modification of crystal shapes during sectioning (cut-section effect); (2) skewing of size distributions to larger diameters due to higher intersection probabilities for large than small particles; and (3) the dependence of the apparent (2D) crystal number density on the orientation distribution of particles (Peterson 1996). Most early studies

* E-mail: jon.castro@oberlin.edu

performed conversions using the method of Wager (1961); more recent studies show this conversion to be inappropriate and suggest more accurate methods (e.g., Hammer et al. 1999, 2000; Higgins 2000; Peterson 1996; Eberl et al. 2002).

In recent studies, 2D data are converted to "true" 3D lengths (or widths) and volume number densities using correction algorithms (e.g., Underwood 1970; Peterson 1996; Sahagian and Proussevitch 1998; Higgins 2000) that minimize errors associated with both the cut-section effect and the intersection probability problem. Despite the common use of these routines, no studies have tested the accuracy of such techniques by comparing CSDs constructed from 2D measurements with corresponding CSDs based on direct 3D measurements. In the present study, we perform such a test by applying these algorithms to intersection lengths of prismatic microlites in obsidian for which we have corresponding 3D size measurements. We use a new technique developed to measure prismatic microlites in samples of low crystallinity (such that the sample is transparent). Our results provide insight on the limitations of stereological conversion methods and for interpretations of CSDs, particularly related to shape variability in natural crystal populations.

3D MEASUREMENT TECHNIQUE

Three-dimensional, crystal-size information may be acquired through serial grinding of rocks, physical extraction of intact crystals (e.g., Dunbar et al. 1994; Bindeman 2003), or by X-ray tomography (e.g., Carlson and Denison 1994). The optical approach described in this section applies to samples in which: (1) crystals are either smaller than a typical thin section thickness (~30 µm), or very well-aligned when viewed in the plane of long-axis orientation; (2) crystal contents are sufficiently low that the sample remains transparent; and (3) crystals are prismatic in form, and approximately equidimensional when viewed perpendicular to their long axes.

We analyzed rhyolitic obsidians from the Inyo volcanic chain, CA. The sample suite consists of: (1) two clasts (OD101 and ODT2) from the northernmost Obsidian Dome tephra lobe (Miller 1985); (2) five samples (OD98) from the western margin of Obsidian Dome (Castro et al. 2002); and (3) one sample (352-6) from glassy margin of the Inyo dike (e.g., Vogel et al. 1989; Table 1). Textural measurements for the five flow-front samples are combined, as their individual size histograms are of similar shape and these samples come from similar positions along the flow margin. All obsidian samples are all finely porphyritic, with approximately 5 vol% phenocrysts comprising **{AU: Note change}** plagioclase, biotite, and hornblende. These sparse phenocrysts are set in a glassy groundmass containing numerous acicular microlites (Fig. 1). Microlites are pseudohexagonal in cross section (Fig. 1b). Reflective light microscopy, TEM studies (e.g., Swanson et al. 1989), and energy dispersive spectroscopy (Castro 1999) show that the microlites are pyroxene. Due to their characteristically narrow widths (~1–2 µm; Table 1), microlites do not produce interference colors in cross-polarized light and, consequently, optical distinction between clinopyroxene and orthopyroxene is not possible.

3D microlite length, width, and number densities were measured in 30 µm thick doubly polished thin sections cut parallel to the plane of flow banding. The measurement technique involves collecting a series of high magnification (1000×) photomicrographs with a digital camera attached to a petrographic microscope. The first image records the upper surface of the thin section, corresponding to the upper focal plane; subsequent images are taken at 1 µm intervals down through the sample to the lower focal plane. These optical serial sections are "stacked" in an image analysis program (NIH *Image 1.62*) to produce an array that is geometrically equivalent to the sequence of slices collected within the thin section. That is, the order in which the images are taken and the position of each slice is preserved in the stack, allowing the analyst to scroll through the series of images. Microlite end points are brought into focus by scrolling through the stack. These end points are labeled when they arrive in focus and assigned a number corresponding to the layer in which the end point resides (Fig. 2). The end point records the x-y position of the microlite whereas the number marks the vertical height of the microlite end point in the volume.

Once all resolvable microlite end points are digitized, the stack of images is averaged into one composite image that preserves both the end point locations and their vertical position numbers. Microlite end points are then connected with a line that represents the two-dimensional, microlite projection length. The averaged image is then thresholded to eliminate all information except these

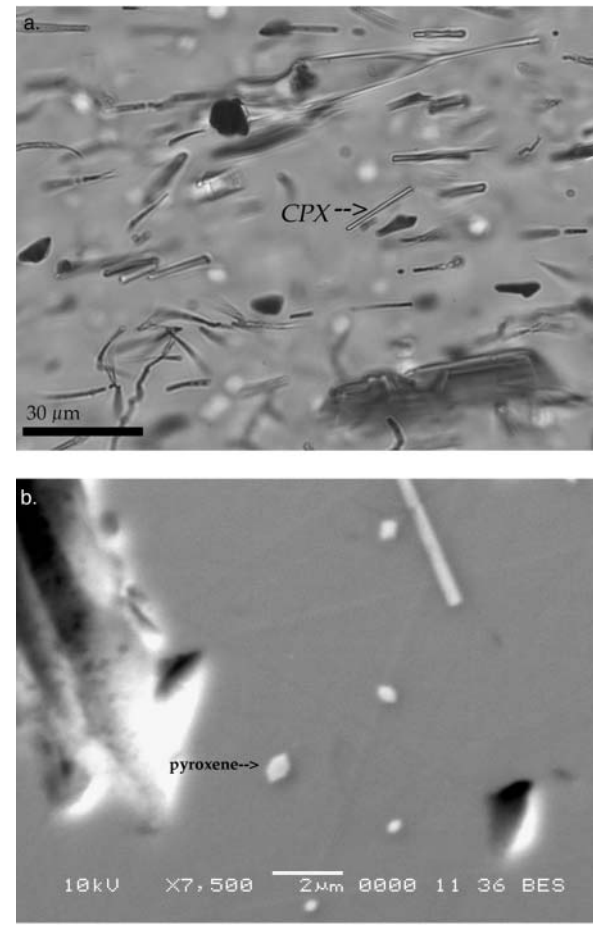

FIGURE 1. (**a**) Photomicrograph of obsidian showing acicular pyroxene **{AU: note change – in the text you state that opx can't be distinguished from cpx; please change on figure also}** microlites in plane-polarized light. Magnification is 1000×. (**b**) Back-scattered electron image of obsidian with microlites evident as polygonal intersections (white) in groundmass glass (gray). Magnification is 7500×.

TABLE 1. Directly measured microlite properties in Inyo obsidians

Sample	No.	Length (µm)		Width (µm)	Aspect ratio	N_V (no/cm³)	Volume fraction
		mean	mode	mean	mean		
ODT2[t]	1185	6.3 (*3.3*)	3.5	1.2 (*0.21*)	4.8 (*3.0*)	1.19×10^9	0.008
OD101[t]	832	5.1 (*3.1*)	3.2	1.2 (*0.34*)	4.3 (*3.6*)	6.16×10^8	0.005
352-6[d]	820	8.2 (*7.0*)	2.5	2.1 (*0.80*)	3.9 (*2.83*)	2.19×10^8	0.008
OD-98[f]	1176	7.0 (*4.1*)	5.5	1.8 (*0.86*)	4.3 (*2.68*)	2.97×10^8	0.005

Notes: t = tephra; d = dike; f = flow front.

lines, whose lengths, orientations (trend angles), and x-y positions are measured using NIH *Image*. The true length of each crystal can then be determined via the Pythagorean Theorem from vertical difference in end point height and the projection length (Fig. 2). Microlite number density is determined by dividing the total number of crystals by the volume analyzed, that is, the area of an image (in μm^2) multiplied by the thickness of the sample, given by the height difference between the first and last image analyzed (in µm). Crystal width is determined in the same manner as projected length, although for acicular crystals (those with prismatic forms), the width does not vary with the orientation of the crystal (i.e., projected width ≅ true width). Thus the vertical position of the width measurement is not important and width can be determined by measurement of projected crystal widths. Microlite volume is calculated from length and width measurements assuming microlites are cylindrical in morphology, with the total volume fraction of microlites being the sum of the individual microlite volumes divided by the volume of sample analyzed.

Measurement error is approximately ±0.1 µm for projection length determinations. High measurement precision is achieved by collecting images at 1 µm intervals. Microlite end points positioned between optical sections are visible, although slightly out of focus, and their position must be approximated. Given this complication, we estimate the uncertainties for vertical positioning of an endpoint to be about ±0.5 µm. Microlites truncated by the upper and lower thin section planes, recognized by their psuedohexagonal and polygonal cross sections (terminations), account for a small percentage (~5%) of all crystals in the analyzed volume. Thus, the length measurements for these few crystals impart an additional but small measurement error on the size distribution.

RESULTS

Microlite dimensions

Measured microlite properties are shown in Table 1. Microlite length is quite variable in all samples, as indicated by large standard deviations about average values. By comparison, microlite width is less variable. Average length is generally larger in dike (8.2 µm) and dome samples (7.0 µm) compared to tephra samples (5.1–6.3 µm). Number density varies from a minimum of about $2.2 \times 10^8/cm^3$ in the dike to approximately $1.2 \times 10^9/cm^3$ in tephra sample ODT2. Microlite volume fractions are low (<0.01) in all samples.

Histograms of microlite length and width for the flow front, dike margin, and tephra are shown in Figure 3. Superimposed on length distributions are lognormal fits to the measured distributions calculated with GALOPER software (Eberl et al. 2002). All length histograms are unimodal and strongly skewed toward large sizes. Two of the length distributions (ODT2, OD98) are lognormal as determined by the chi-squared test, one sample (OD101) is nearly lognormal but fails the chi-squared test, and one sample (352-6) has an asymptotic distribution (Eberl pers. comm.). Modal length varies among the sample suite, with the largest modes (5.5 µm, 3.5 µm) recorded in the two samples with lognormal length distributions (ODT2 and OD-98), and the smallest modal length (2.5 µm) recorded in the dike sample (352-6). Microlite width distributions are symmetrical and display modes ranging from approximately 2 µm in samples 352-6 and OD98 to about 1.2 µm in samples (OD101) and (ODT2).

Microlite aspect ratio (A; long/short dimension) **{Au: Note that bold italics is reserved for matrices}** exhibits a wide range in all samples (Table 1), as illustrated for sample OD101 in Figure 4a. The range in A is broad, varying by a factor of nearly 30 within this sample. Most (>90%) of the population, however, varies over one order of magnitude in A, with habits ranging from equant (A = 1) to elongate (A = 10). Like the length distribution (Fig. 3), the aspect ratio histogram is strongly

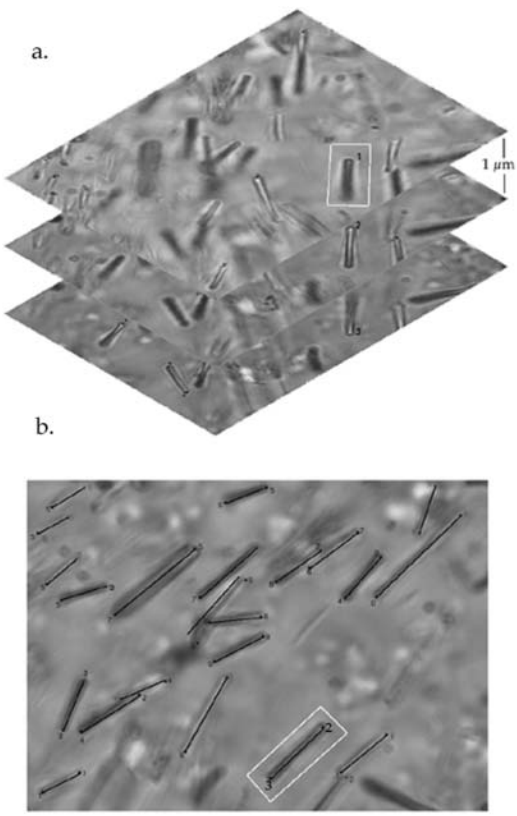

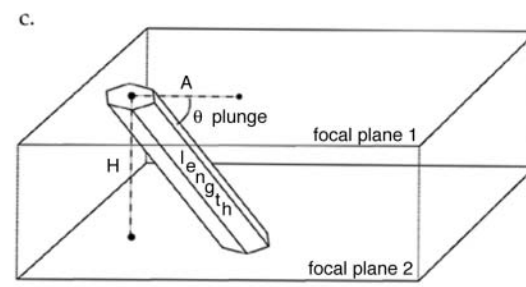

FIGURE 2. Microlite measurements are made on a series of optical slices with the program *NIH Image*. (**a**) Image stack consisting of three images collected at 1 µm intervals. Microlite end points are labeled in each image with a dot and a number corresponding to their vertical position in the stack. (**b**) An average of all individual images in the stack. On this image, black lines are drawn to connect the microlite end points thus providing a measure of the projected length. Numbers reflect the vertical position of microlite end points in the stack. The program measures the lengths of the sticks while the difference in microlite end point height is entered in a spreadsheet. (**c**) Calculation of true length and plunge use the projection length (P) **{AU: Note change; "A" was used already for aspect ratio, so you must use another abbreviation here; also, change on figure}** and end-point height difference (H) measurements determined from image analysis.

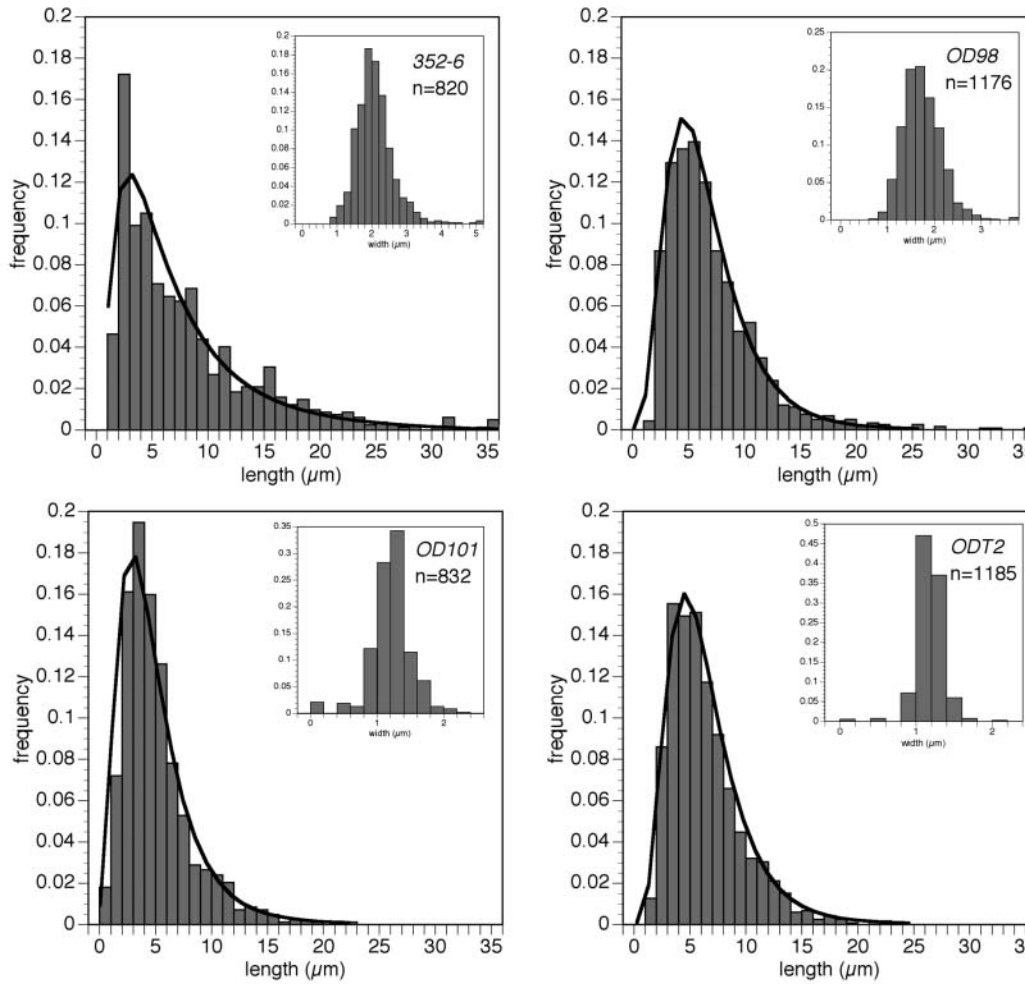

FIGURE 3. Histograms of microlite 3D length and width (insets). All length distributions are skewed toward large size whereas width is normally distributed. Solid curves are lognormal fits to size distributions. Length distributions for samples OD98 and ODT2 are lognormal whereas samples 352-6 and OD101 are asymptotic and nearly lognormal, respectively. The mode of OD101 is displaced slightly to the right of position expected for the theoretical lognormal curve (Eberl, pers. comm.).

skewed to the right. This asymmetry reflects the positive correlation between *A* and crystal length (Fig. 4b). The data in Figure 4b are bounded on either side by lines of constant crystal width (from 0.4 to 2 μm). Variations in *A* thus reflect changes in both length and width. As would be expected from the inverse relationship between width and *A*, the maximum in *A* generally decreases with increasing width (Fig 4b. inset), defining a negatively sloping envelope on the upper part of the data array. The range in *A* also decreases with increasing width.

There are two important implications of the *A* variations depicted in Figure 4. First, these variations suggest that the long and short crystallographic directions both experienced a range of growth rates during the crystallization interval. Had the growth rates remained constant, only one shape would be generated. It is difficult to decipher, however, from the *A* data of a single sample alone, how the shape population may have evolved with time under conditions of variable growth rate. For example, the observed shape population could have been produced by relatively rapid growth of the long crystal dimension followed by subsequent "thickening" of many early formed long slender crystals by protracted growth of the width dimension (e.g., Hammer et al. 1999). In this scenario, the few highly elongate and slender crystals plotting to the right in Figure 4b are remnants of a shape population that has shifted to lower aspect ratios by later growth of the width dimension. Alternatively, the shape distribution could have been influenced by varying degrees of resorption of the long and short crystal dimensions. The resorption mechanism seems unlikely however, due to the euhedral character of microlites and the absence of resorption textures. If, indeed, crystals grew over a range of rates, then CSD models that assume a constant growth rate (e.g., Marsh 1988; Cashman and Marsh 1988) should be modified to account for variable growth (e.g., Eberl et al. 2002).

Another important implication of *A* variations relates to the manner in which stereological correction programs convert 2D intersection length to 3D CSDs (e.g., Higgins 2000; Peterson

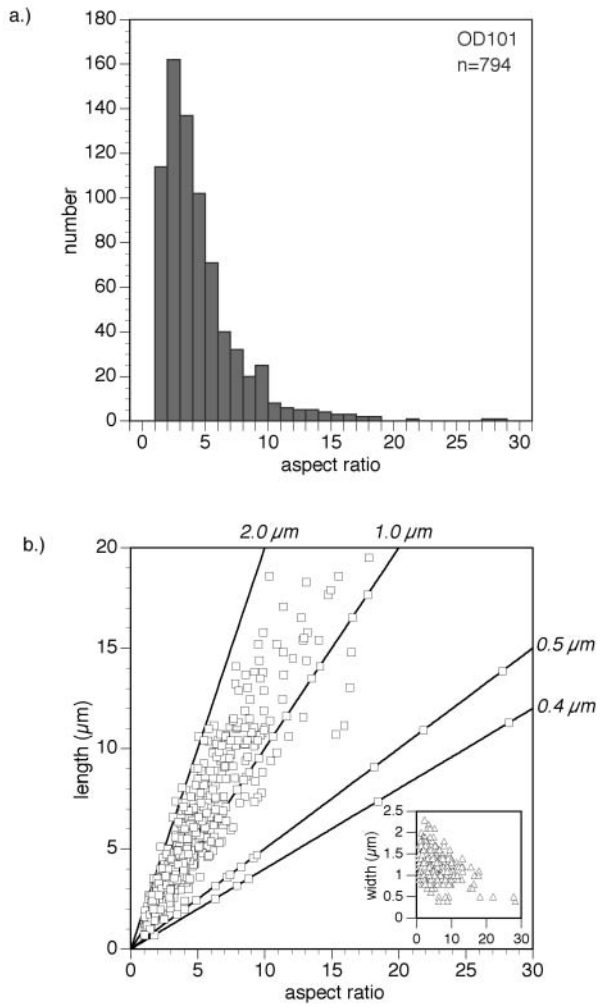

FIGURE 4. (**a**) Aspect ratio (*A*) histogram for sample OD101. (**b**) Length (squares) and width (triangles) vs. aspect ratio. This plot illustrates the strong correlation between length and aspect ratio and a negative diffuse correlation shown by width (inset). Numbered lines in *A* vs. length represent constant width populations (i.e., slope = width). Along these lines aspect ratio varies due to relatively rapid growth of the long crystallographic dimension. The range in *A* is large for small width values, and appears to diminish as width increases (Fig. 4b inset). Variations in the growth rates of both long and short axes may produce the observed *A* distribution.

1996; Sahagian and Proussevitch 1998). As these methods assume that crystal-shape populations are self-similar, application of these techniques requires a one-to-one correspondence between the intersection dimension and the true dimension (e.g., Higgins 1994). The microlite shape distribution demonstrates, however, that a single intersection length may in fact correspond to a range of true lengths (Fig. 4b inset). Below we investigate the degree to which these shape complications affect the performance of three commonly used stereological correction routines as applied to prismatic crystals with a range of aspect ratios.

Crystal size distributions from direct measurements

3D CSDs were constructed from measurements of true length (*L*) and analysis volume. CSDs depict the natural logarithm of the population density (*n*) vs. length (e.g., Cashman and Marsh 1988; Marsh 1988), where *n* is defined as the number of crystals per unit volume within a particular size interval, or:

$$n = \mathrm{d}N/\mathrm{d}L \quad (1)$$

N is the cumulative number of crystals with length ≤*L*, per unit volume. Binning of data into 2 μm intervals provides both sufficient detail at small crystal sizes and smooth plots at large crystal sizes. Figure 5 shows CSDs for all four samples. CSDs are linear over most of the measured size range (1–30 μm). Departure from linearity is evident in the two samples with lognormal length distributions (ODT2 and OD98) for crystal sizes ≤6 μm, where the population density drops below the linear trend demarcated by larger crystals. The other two samples (352-6 and OD101) have a less-pronounced downturn at $L \leq 4$ μm. Because our optical system measures crystals ≥0.5 μm, these departures from linearity are considered to be real and not an artifact resulting from poor measurement resolution.

The intercepts and slopes of linear CSDs have been used to estimate a number of textural characteristics in a crystal population; relative changes in these parameters have led to interpretations regarding the conditions of crystal nucleation and growth (e.g., Cashman and Marsh 1988). These interpretations rest on the assumption that the crystal growth rate is constant, which is generally not known *a priori*. Although there is evidence in microlite shape distributions (Fig. 4) and in the lognormal forms of two size distributions (Fig. 3; Eberl et al. 2002) that microlite populations grew at variable rates, it is still instructive to compare CSD-derived textural parameters determined using an assumption of constant growth (e.g., Marsh 1988) with corresponding values determined with direct 3D measurements. Such comparisons allow us to assess whether accurate textural information can be extracted from a linear size distribution regardless of the inferred growth model.

CSD slopes and intercepts, along with descriptions of the CSD shapes, are summarized in Table 2. CSD intercepts range from a maximum of 1.6×10^{13}/cm^4 in sample ODT2 to a minimum of 5.9×10^{11}/cm^4 in sample 352-6. Accompanying this drop in intercept is a reduction in CSD slope (Table 2). Assuming that crystals grow at the same rate, the dominant length (L_D) of a crystal population with a log-linear **{AU: Is this correct?}** CSD can be determined as the inverse of the CSD slope (slope = $1/L_D$; e.g., Marsh 1988). For example, the relatively steeply sloping CSDs of samples ODT2 and OD101 reflect smaller dominant lengths (3.0–3.3 μm) compared to samples OD98 (L_D = 4.2 μm) and 352-6 (L_D = 5.9 μm), which have shallower CSD slopes (Table 2). CSD-derived L_D for samples ODT2 and OD101 closely match their respective modes in directly measured distributions (Table 1 and 2). In contrast, L_D overestimates the mode of sample 352-6 by a factor of two, and somewhat underestimates the mode of sample OD98. L_D for sample 352-6 (5.9 μm) rather closely matches the median length (6.2 μm).

CSD intercepts provide a measure of the nucleation density (n^o), or the theoretical number of nucleus-sized crystals in the population. This parameter is obtained by extrapolating the linear CSD trend defined by the larger crystals. Although hypothetical, n^o can be combined with L_D to derive other textural

TABLE 2. Microlite properties calculated from regressed CSDs assuming constant-rate crystal growth

Sample	No.	CSD form*	ln n (/cm^4)	n^o (/cm^4)	Slope	L_D (μm)	N_T (/cm^3)	Volume fraction
ODT2[t]	1185	lognormal	29.6	7.16×10^{12}	–0.305	3.3	2.36×10^9	0.009
OD101[t]	832	near-lognormal	28.5	2.38×10^{12}	–0.302	3.3	7.85×10^8	0.005
352-6[d]	820	asymptotic	26.8	4.36×10^{11}	–0.170	5.9	2.57×10^8	0.01
OD98[f]	1176	lognormal	27.4	7.94×10^{11}	–0.238	4.2	3.33×10^8	0.005

Notes: t = tephra; d = dike; f = flow front.
* CSD form determined by chi-squared analysis (Eberl, pers. comm.)

characteristics, such as the total number density (N_T) of crystals in a sample volume ($N_T = L_D n^o$). N_T values in all samples are similar **{AU: Note change}** to number densities (N_v) determined from direct measurements (Tables 1 and 2). The largest difference between N_v and N_T occurs in sample ODT2, in which N_T is about twice the directly measured number density. The difference is likely related to the marked downturn of the CSD at small sizes, which reflects a paucity of small crystals ($L < 6$ μm), and to N_T being an extrapolation to very small crystals. Although similar discrepancies can be seen in samples OD98, 352-6, and OD101, in most cases, the CSD-derived number density overestimates the measured number density by <20%.

Microlite volume fractions (V) can be calculated from CSD parameters using the formulation presented in Marsh (1988):

$$V = 6\sigma n_o L_D^4 \quad (2)$$

Here, σ is a shape factor calculated from the average crystal shape (i.e., the long, intermediate, and short dimensions) and roundness of the crystals measured, and L_D is the dominant length determined from the CSD slope. Microlite volume fractions determined in this manner closely match those from direct measurements (Tables 1 and 2). The slight overestimate of crystal-volume fraction for sample 352-6 may result from the assumption of an average shape factor, as this sample exhibits the largest variation in length (Table 1).

In summary, textural information derived from linear CSDs using formulations (e.g., Marsh 1988) based on the assumption of constant crystal growth appears accurate despite evidence that crystal growth was not constant (Eberl et al. 2002). Thus, our comparisons show that, at least for the growth dispersion (i.e., growth at variable rates) experienced by the crystals within these obsidian samples, N_T and V may be estimated from the geometry of linear CSDs alone, independent of the assumption of a governing crystal growth law (e.g., constant vs. size-proportionate growth).

Construction of CSDs from 2D intersection data

High crystal-volume fractions in most igneous rocks limit measurements to 2D thin sections, and thus conversion to 3D requires stereological corrections (e.g., Underwood 1970; Peterson 1996; Sahagian and Proussevitch 1998; Higgins 2000). To assess the accuracy of stereological conversion routines, we applied the techniques of Underwood (1970), Peterson (1996), and Higgins (2000) to correct a series of 2D microlite intersection length measurements for which we have corresponding 3D measurements. Intersection length was measured as the longest dimension of the microlite exposed in reflected light images of sample OD101 (Table 3). Microlites in this sample have a mean aspect ratio of 4.2 ($n = 633$) and appear to be randomly oriented (Table 1). We did not use the stereological conversion of Sahagian and Proussevitch (1998) as their technique: (1) was developed for measuring vesicles with small aspect ratios and a limited range of shapes, and (2) requires particle counts of more than 10^2 for each size class and total counts of about 10^4 to ensure accurate tailing corrections (Proussevitch 2002; personal communication)**{{Au: Does the notation 'personal communication' refer to Proussevitch (2002)? If so, please delete the date, as it leads the reader to believe a paper is being cited. If not, please provide a reference for Proussevitch (2002).}}**. The thin section data included in this study contain too few measurements (~600 crystals), especially in the largest size bins, for statistically valid treatment with their algorithm. Additionally, the time required to make statistically viable counts in the largest size classes would greatly exceed the time needed to perform the manual 3D measurements.

Errors in the conversion of 2D measurements to 3D arise from: (1) the sectioning of crystals along dimensions smaller than their greatest length (cut-section effect), and (2) the intersection-probability effect whereby small crystals are intersected less often than large crystals. Additional errors may originate from the presence of crystal preferred orientations (CPO), which affect the number of crystals exposed in the sample plane (Peterson 1996). Corrections for the cut-section effect are based on an approach developed by Saltikov (1967). In this method, the largest intersections of the population are used as reference for calculating successively smaller size classes, which contain contributions from the larger classes in addition to crystals that truly belong in the size class of interest. The accuracy of this correction depends on a statistical representation of each 2D class produced by random intersection of each 3D class. Counting errors become substantial for the largest size classes, which commonly have the lowest number densities. Further complications arise when measuring elongate particles, whose intersection probability along the long axis is small compared

TABLE 3. Intersection data on sample OD101 used to construct Figure 6

Length (μm)	No.
0.5	0
1.0	460
2.0	144
3.0	8
4.0	9
5.0	3
6.0	2
Shape	4.2
Area (μm^2)	41772
Roundness	0
Fabric	massive

Notes: "Length" is the intersection length and given values mark the lower limit of each interval. "Shape" is the average aspect ratio determined from 3D measurements.

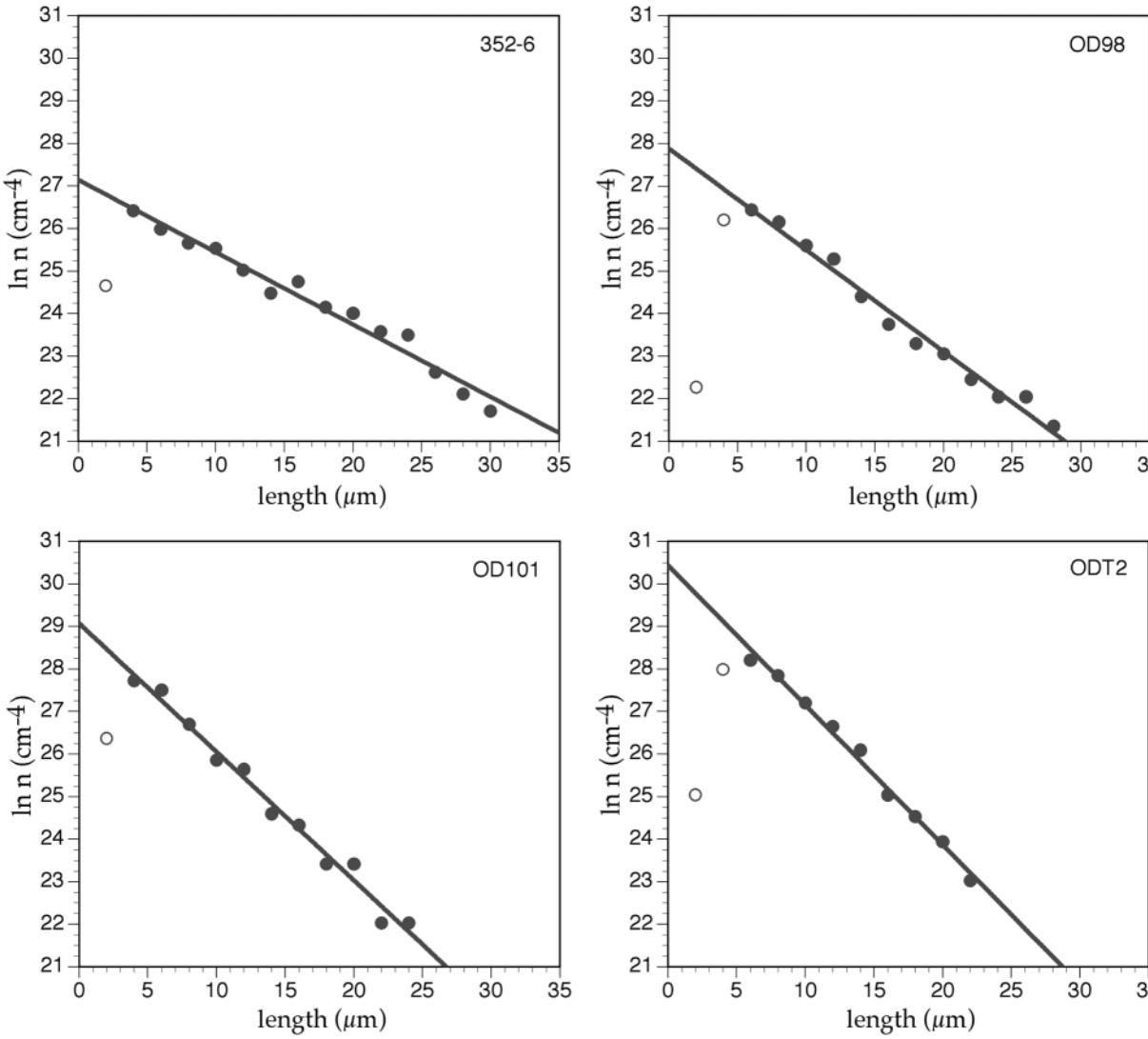

FIGURE 5. Crystal-size distributions constructed from 3D length measurements and the natural log of the population density (n). All CSDs are linear over most of the size range and show a downturn at small lengths. Downturns are real features of these populations as measurement resolution is ~0.5 μm. Linear regressions are best fits to CSD data and have minimum R^2 values of 0.97.

to the shorter dimensions (e.g., Fig. 6 in Sahagian and Proussevitch 1998). The intersection probability effect can be accounted for by converting the crystal area number density (N_A) to the volumetric number density (N_V) with the relation: $N_V = N_A/d$, for each bin size d (Underwood 1970). This correction does not account for the cut-section effect and preferred grain alignments. The Higgins (2000) conversion routine is a form of the Saltikov (1967) technique with modifications to correct for crystal shape and the geometry and overall strength of CPO fabrics. In contrast, the method of Peterson (1996) assumes that the crystal population conforms to a lognormal size distribution and fits the intersection data using a statistical approach. The Peterson (1996) technique also makes corrections for crystal shape and the strength and nature of CPO.

To avoid errors related to complex crystal shapes and low particle counts in the large size bins, the Higgins and Peterson algorithms both use the mode of the intersection length distribution to convert intersection length to true length and number density. For example, the modal intersection length of a prismatic crystal cut by many randomly oriented planes corresponds to the short dimension, S (Higgins 1994; Sahagian and Proussevitch 1998). Using this relation, and assuming that shape is constant, Higgins (2000) converts intersection length (l_{int}) to true length (L) by way of: $L = l_{int} * (L/S)$. L/S, the average aspect ratio (A), is generally determined from analysis of intersection width to length ratios measured in 2D (e.g., Higgins 1994; Hammer et al. 1999). The Peterson (1996) algorithm follows a similar approach to convert the measured l_{int} to L: $L = l_{int} * k * A$. k is a scale factor (≈1 for elongate prisms; Peterson 1996) and A is the intersection aspect ratio. CSDs constructed with the Underwood (1970) correction require a similar procedure for converting l_{int} to L, namely, $L = l_{int} A$. In this study, we

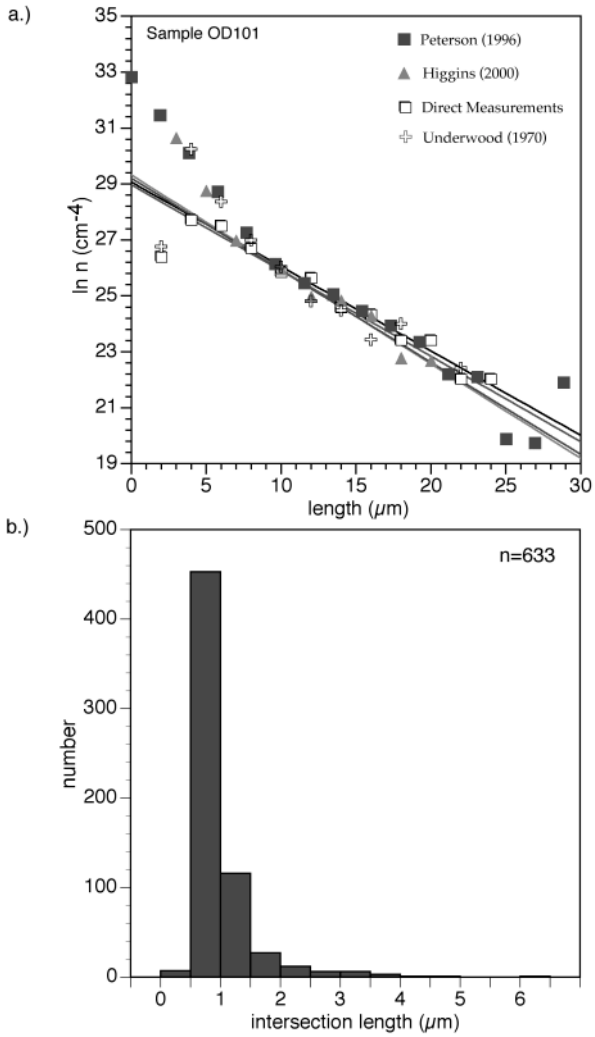

FIGURE 6. (**a**) Comparison of CSDs in sample OD101 derived from intersection lengths (**b**) using the correction routines of Higgins (2000; solid triangles), Peterson (1996; solid squares), Underwood (1970; open crosses), and direct 3D measurements (open squares). The Underwood, Higgins, and Peterson CSDs match the real distribution for $L > 7$ μm, however, they depart for smaller sizes showing relatively large population densities. The distribution calculated using the Underwood method incorporates a similar shape correction, where the intersection length is converted to true length by the average aspect ratio (see text). The appearance of a kink in CSDs produced by these methods suggests that aspect ratio variations lead to systematically high population densities and nonlinear CSDs.

determined a range of *A* from direct measurements (Fig. 4; Table 1), and used the average value for CSD calculations.

Figure 6 shows CSDs of sample OD101 generated using the simple algorithm of Underwood (1970), *CSD corrections 1.2* of Higgins (2000), and the algorithm of Peterson (1996) as obtained from his website (www.nrcan.gc.ca/~tpeterso/csd_e.html). The CSD obtained from direct measurements is shown for comparison. For each CSD, regression lines were fitted to linear segments that span the largest size range. For example, the CSD constructed using the Peterson (1996) technique is kinked at approximately 9 μm and thus the five smallest bins, in addition to the three largest size bins, which fall off the linear trend, were omitted from the regression. Similarly, we omitted the two smallest size bins from the regression of the CSD produced with *CSD corrections*. CSD slopes, intercepts, regression coefficients, and other parameters are listed in Table 4.

All three calculated CSD trends match the real 3D distribution over a large portion of the measured size range (Fig. 6a). The Higgins-derived CSD closely approximates the true distribution over the size range from 7 to 20 μm, whereas the Peterson-derived CSD matches the true distribution from about 8 to 24 μm. The CSD derived from the Underwood (1970) calculation, although not as smooth, is similar in slope, intercept, and overall form to the CSDs produced using the Peterson and Higgins techniques. Algorithm-based CSD slopes differ only slightly from the directly measured CSD between ~7 and 24 μm, corresponding to small differences in the dominant length (Table 4). However, these slope differences translate to errors in CSD intercept (i.e., ln *n*) of about 0.8 log units or approximately 13%. The overall kinked shapes of these plots differ from the form of the real CSD, which is linear over most of the size range.

The Underwood, Higgins, and Peterson-derived CSDs show a break in slope between 7 and 9 μm, marking a sharp increase in the population density for the smaller size classes. The points of inflection differ among these CSDs owing to slightly different bin sizes. It is likely that the sharp rise in ln (n) at $L < 7$ μm represents systematic error that stems from aspect ratio variability in the crystal population. These aspect ratio variations go "undetected" because the correction routines use a fixed aspect ratio to convert all intersection measurements. Consequently, large positive errors in number density result for size classes containing crystals with relatively constant short dimensions but highly variable lengths (Fig. 4b, inset). Indeed, the close match between the Underwood-derived CSD, which accounts solely for intersection probability and assumes a one-to-one correspondence between intersection and true lengths, is evidence that errors are primarily due to significant shape variability in the real population.

Although errors in ln (*n*) are large for $L < 7$ μm for all three conversion techniques, there is a close match between calculated and real CSDs for $L > 7$ μm. Thus, all three methods appear to work quite well for larger crystal sizes, and all three provide reasonably accurate estimates of both dominant crystal size and total crystal number density. Interpretation of CSD trends is more problematic when plots are not linear. Kinked and curved CSDs in magmatic rocks have been interpreted to represent mixed crystal populations (Armienti et al. 1994; Higgins 1996), sharp variations in growth and/or nucleation

TABLE 4. CSD parameters determined with correction algorithms and assuming a constant growth model

Method	ln *n* (/cm^{-4})	Slope	R^2	L_D (μm)	N_T (/cm^3)
Direct measurements	28.5	–0.30	0.98	3.3	7.9×10^8
Higgins	29.3	–0.33	0.96	3.0	1.6×10^9
Peterson	29.2	–0.33	0.98	3.0	1.4×10^9
Underwood	28.9	–0.31	0.91	3.2	1.1×10^9

rate (Marsh 1998), or crystal-settling phenomena (Peterson 1996). However, as the apparent kinks in our calculated CSD curves are clearly an artifact of assuming a constant crystal shape, we suggest that interpretations of non-linear CSD trends should be made with caution.

It is difficult to assess whether shape variability is important in other magmatic systems, as information on 3D crystal shape variability in magmatic rocks is scarce. Hammer et al. (1999) measured minor (less than a factor of two in 2D) apparent aspect ratio variations for prismatic and tabular plagioclase microlites in a sequence of dacitic pyroclasts from Mt. Pinatubo. Their CSDs, constructed from 2D measurements using the Peterson correction technique, were mostly linear, suggesting that small variations in crystal shape do not strongly influence the results of the conversion routine. This observation, coupled with our finding that widely varying aspect ratio may induce systematic errors, highlights the importance of assessing crystal-shape distributions in samples selected for CSD analysis. Unfortunately, there is no way to determine the absolute range and distribution of shape classes in a volume without performing tedious 3D measurements via serial sectioning, physically extracting crystals for measurement, or employing tomographic imaging techniques.

CSDs constructed from 2D projection lengths

Although 3D crystal-size measurements are the preferable way of characterizing a crystal population, the measurements are time consuming and thus limit the number of samples that can be analyzed. For this reason, we have explored the possibility of using apparent crystal lengths to approximate 3D crystal measurements. Microlite dimensions in our obsidian samples are typically less than the thickness of a standard thin section (~30 μm). Under these circumstances, the apparent length of a prismatic microlite projected onto the surface of the thin section, its projection length, provides a more-reliable estimate of true length than the intersection dimension. Projection length depends on the plunge of a microlite relative to the plane of the thin section. When plunge is zero (i.e., the crystal is horizontal), projection length equals the true length. The difference between true and projected length increases with the plunge angle. Accurate CSDs can therefore be determined from measurements of projection length alone provided that microlites are well aligned within the plane of the thin section.

In obsidian samples, we find that thin sections cut within the plane of flow lamination in many cases **{AU: Note change}** expose shallowly plunging microlites, as flattening fabrics are common in obsidian lavas (e.g., Manga 1998; Castro et al. 2002). Well-developed flow laminations are less common in tephra obsidians of the Inyo system. In general, microlites exhibit large orientation scatter due to vesiculation, complex flow histories, and deflection of microlites around larger crystals. Consequently, CSDs based on true and projection length will differ depending on both orientation variability and the orientation of the thin section.

Here we examine the effects of microlite orientation variability on projection length-based CSDs for a tephra sample (ODT2). The orientation (plunge angle) distribution of microlites in sample ODT2 is shown in Figure 7a. About 26% of the microlites are aligned within the plane of the thin section (e.g., plunge <5°), but as the orientation distribution shows, there is significant variability in plunge. The differences between true and projection length **{AU: For consistency, changed to "projection length" (here and elsewhere)}** are small (<6%) for microlites plunging less than 20°. Errors increase with the plunge angle. Figure 7b shows microlite true length plotted against normalized projection length for sample ODT2. Approximately 78% of the data fall within 0.1 projection length unit of the horizontal line where the true length equals the projection length. Scatter below this line arises from microlite plunge variability in the plane of the thin section. This scatter is organized into distinct splays off the linear trend, each of which corresponds to a group of microlites with the same end point height difference. These groupings are clearly an artifact of our 1 μm optical sampling interval and the assignment of end-point height to specific optical sections. In the real population, microlite tips are distributed over a continuum of vertical positions.

We compare CSDs for sample ODT2 based on projection and true lengths in Figure 8. Despite the scatter in orientation (e.g., Fig. 7a), there is a close correspondence between true and projection length-based CSDs, a correspondence attributable to both the high degree of crystal alignment and the large number (>10^3) of crystals measured. Linear fits to these data show negligible differences in CSD slope and intercept (<2%). Departure from the 3D CSD occurs in the smallest size class (L < 2 μm), where the population density of projection lengths exceeds the 3D lengths by about one log unit. This discrepancy may reflect higher orientation (plunge) scatter in smaller crystals, which tend to have smaller aspect ratios (Fig. 4b). In a simple shear flow, crystals of small aspect ratio will move more slowly and rotate with higher period than those with large aspect ratio (Jeffrey 1922; Manga 1998), thus requiring larger strains to achieve alignment. As the projection length is determined by microlite plunge, the apparently large number of crystals in the small size class could reflect these orientation effects.

In summary, CSDs based on projection length may serve as accurate records of the crystal population in obsidian, provided that microlites are moderately well-aligned and thin sections are cut parallel to the direction of alignment. If microlites are not well-aligned, errors will arise due to the effects of variable microlite plunge on the resultant CSD.

Discussion and Concluding Remarks

In this paper, we presented a method for measuring the true length and number density of acicular microlites in rhyolitic obsidian. Whereas the measurement technique presented here is moderately labor and time intensive (~60 crystal measurements/hr), the data acquired are of high quality and thus useful for making an accurate textural characterization. CSDs also may be constructed on the basis of projection length, provided that samples have well-developed microlite preferred orientations (e.g., lineations or alignment within the foliation plane). Under these conditions, thin sections cut parallel to the fabric minimize differences between projection and true length.

3D size and shape distributions of pyroxene microlites in obsidian provide insight into the early stages of magmatic crys-

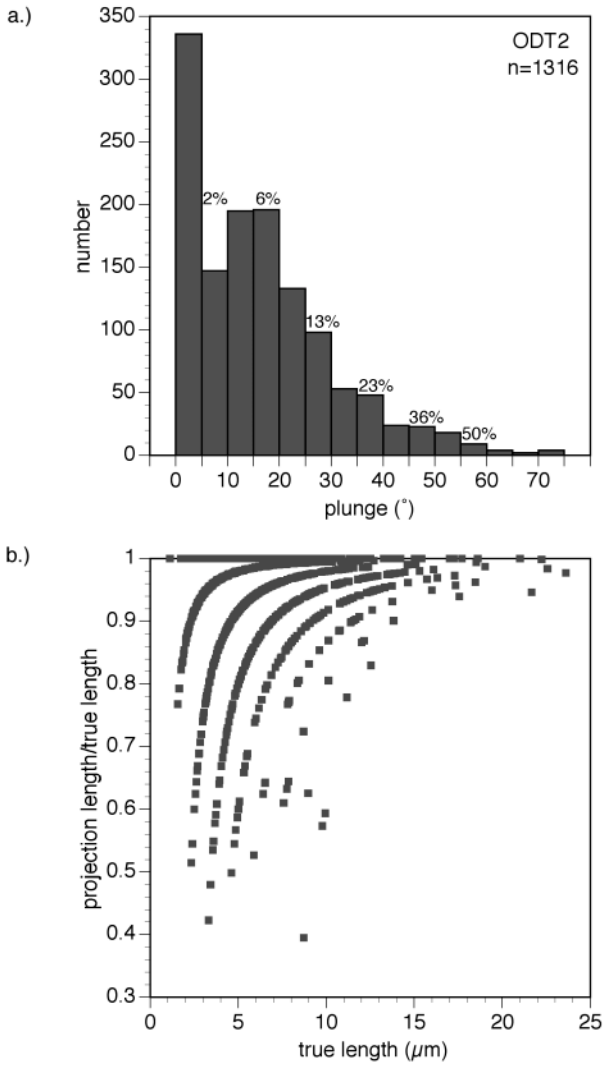

FIGURE 7. (**a**) Histogram showing the plunge-angle distribution for microlites in sample ODT2. Percent values indicate the difference between true and projection length for microlites within a given range of plunge. For example, the projection length for microlites within the plunge = 5–10° will be about 98% of the true length (i.e., a 2% difference). Note that most of the microlites in this sample have shallow plunge and consequently projection-length measurements will closely approximate the true length distribution. (**b**) Plot of true length vs. normalized projection length for sample ODT2. The scatter falling below the linear trend reflects the difference between projection length and 3D length arising from microlites plunging out of the plane of measurement. Individual splays of data off the linear trend correspond to groups of microlites with a specific end-point height differences (e.g., 1 μm, 2 μm, 3 μm, etc.). For example, the first splay, represents all microlites with an end point height difference of 1 μm. Each successive array (toward the RHS of the diagram) corresponds to a progressively larger end-point height difference (e.g., 2 μm, 3 μm, 4 μm, etc.). Microlite plunge is greatest at the end of each splay, where the end-point height difference approaches the true length of the crystal, and gets progressively smaller where the splay converges with the linear trend.

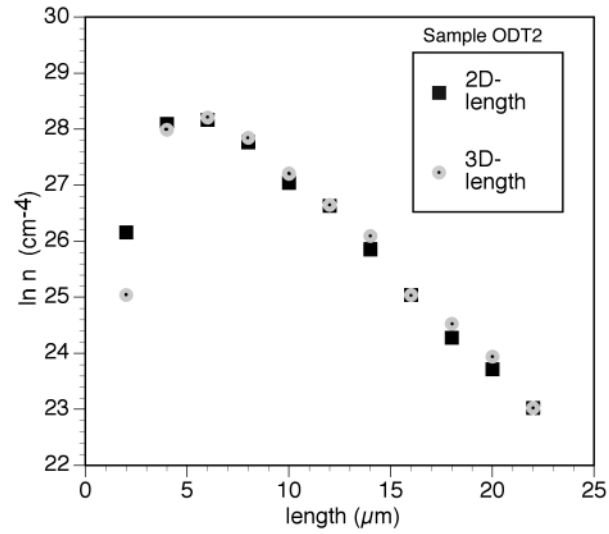

FIGURE 8. CSDs based on true length (dotted circles) and projection length (solid squares). The CSD parameters (e.g., L_D, N_T, n^o) derived from these plots under the assumption of constant crystal growth rate (e.g., Marsh 1988), differ by less than 2%. CSDs based on projection length may be good approximations of the true CSD provided that microlites are well-aligned (i.e., shallowly plunging) within the plane of measurement.

tallization. The broad range of aspect ratios exhibited in shape distributions suggests variable crystal growth rates. An outcome of this growth dispersion is the development of lognormal and asymptotic size distributions during the initial stages of crystallization. These linear CSDs may evolve with time to progressively more curved and normal size distributions (Castro 1999) if the governing growth law shifts to one involving constant-rate growth (e.g., Eberl et al. 2002), or if the system changes from early nucleation-dominated behavior to a growth-dominated system (e.g., Hammer et al. 1999). Despite the evidence for variable crystal growth rates, interpretations of linear CSD based on models that assume constant growth may still yield accurate textural information, as shown by the correspondence between directly measured and CSD-derived textural parameters.

The three dimensional CSDs based on direct measurements allow us to test theoretical formulations for converting 2D intersection length and area number density to CSDs. Our comparisons indicate that CSDs produced with the Underwood (1970), Higgins (2000), and Peterson (1996) techniques closely match the true distribution over a limited size range (~7–25 μm), and for $L < 7$ μm, calculated CSDs depart from the true distribution, resulting in a kinked form. The large positive errors in population density that accompany the break in CSD slope arise as artifacts related to significant shape (aspect ratio) variability in the population. Thus, textural parameters (e.g., L_D and N_T) derived from CSD regressions of these crystal populations may be inaccurate and interpretations of underlying magmatic processes may be misleading. In light of complications arising from shape variability, inferences regarding magmatic processes (e.g., mixing, crystal settling, crystallization kinetics) based on CSD morphology should be coupled with

an assessment of crystal-shape variability. Where possible, CSDs of acicular microlites should be constructed on the basis of 3D measurements, provided samples are of sufficiently low crystallinity and crystals are generally smaller than the thickness of the thin section.

ACKNOWLEDGMENTS

This work was supported by NSF Grant EAR-9805305. The authors are grateful to A. Proussevitch, who provided the numerical code of Sahagian and Proussevitch (1998) and offered helpful advice on the use of the stereology formulation. The comments by D. Sahagian, M. Higgins, and D. Eberl greatly improved this manuscript. Authors also thank T. Vogel, for providing thin sections of the Inyo dike. C. Mercer helped measure microlites in the Inyo tephra samples.

REFERENCES CITED

Armienti, P., Pareschi, M.T., Innocenti, F., and Pompilio, M. (1994) Effects of magma storage and ascent on the kinetics of crystal growth. Contributions to Mineralogy and Petrology, 115, 402–414.

Bindeman, I.N. (2003) Crystal sizes in evolving silicic magma chambers. Geology, 31, 667–670.

Carlson, W.D. and Denison, C. (1994) Mechanisms of porphyroblast crystallization: results from high-resolution computed X-ray tomography. Science, 1236–1239. **{{Author Query: Please provide the issue number for this paper.}}**

Cashman, K.V. (1990) Textural constraints on the kinetics of crystallization of igneous rocks. In J. Nicholls and K. Russell, Eds., Modern methods of igneous petrology: Understanding magmatic processes. Mineralogical Society of America, Reviews in Mineralogy, 24, p. 259–314.

——— (1992) Groundmass crystallization of mount St. Helens dacite, 1980-1986: a tool for interpreting shallow magmatic processes. Contributions to Mineralogy and Petrology, 109, 431–449.

——— (1993) Relationship between plagioclase crystallization and cooling rate in basaltic melts. Contributions to Mineralogy and Petrology, 113, 126–142.

Cashman, K.V. and Marsh, B.D. (1988) Crystal size distribution (CSD) in rocks and the kinetics and dynamics of crystallization II. Makaopuhi lava lake. Contributions to Mineralogy and Petrology, 99, 292–305.

Cashman, K.V., Kauahikaua, J.P., and Thornber, C. (1999) Cooling and crystallization of lava in open channels, and the transition of pahoehoe lava to a'a. Bulletin of Volcanology, 61, 306–323.

Castro, J.M. (1999) Textural and structural development of obsidian lavas. Ph.D. dissertation. University of Oregon, 163 pp.

Castro, J.M., Manga, M., and Cashman, K.V. (2002) Dynamics of obsidian flows inferred from microstructures: insights from microlite preferred orientations. Earth and Planetary Science Letters, 199, 211–226.

Dunbar, N.W., Cashman, K.V., and Dupre, R. (1994) Crystallization processes of anorthoclase phenocrysts in the Mount Erebus magmatic system; evidence from crystal composition, crystal size distributions, and volatile contents of melt inclusions. In P.R. Kyle, Ed. Volcanological and environmental studies of Mount Erebus, Antarctica, 66, p. 129–146. American Geophysical Union, Washington, DC, United States.

Eberl, D.D., Kile, D.E., and Drits, V.A. (2002) On geological interpretations of crystal size distributions: Constant vs. proportionate growth. American Mineralogist, 87, 1235–1241.

Hammer, J.E., Cashman, K.V., Hoblitt, R.P., and Newman, S. (1999) Degassing and microlite crystallization during pre-climactic events of the 1991 eruption of Mt. Pinatubo, Philippines. Bulletin of Volcanology, 60, 355–380.

Higgins, M.D. (1994) Determination of crystal morphology and size from bulk measurements on thin sections: numerical modeling. American Mineralogist, 79, 113–119.

——— (1996) Crystal size distributions and other quantitative textural measurments in lavas and tuff from Mt Taranaki (Egmont volcano), New Zealand. Bulletin of Volcanology, 58, 194–204.

——— (2000) Measurement of crystal size distributions. American Mineralogist, 85, 1105–1116.

——— (2002a) Closure in crystal size distributions (CSD), verification of CSD calculations, and the significance of CSD fans. American Mineralogist, 87, 171–175.

——— (2002b) Closure in crystal size distributions (CSD), verification of CSD calculations, and the significance of CSD fans: reply. American Mineralogist, 87, 1242–1243.

Jeffrey, G.B. (1922) The motion of ellipsoidal particles immersed in a viscous fluid. Proceedings of the Royal Society of London A, 102, 161–179.

Lasaga, A.C. (1998) Reaction kinetics in geoscience. Princeton University Press, Princeton, 811pp. **{{Author Query: This paper is not cited in the text. Please either insert a citation or remove the reference.}}**

Manga, M. (1998) Orientation distribution of microlites in obsidian. Journal of Volcanology and Geothermal Research, 86, 107–115.

Mangan, M. (1990) Crystal size distribution systematics and the determination of magma storage times: Ther 1959 eruption of Kilauea volcano, Hawaii. Journal of Volcanology and Geothermal Research, 44, 295–302.

Marsh, B.D. (1988) Crystal size distributions (CSD) in rocks and the kinetics and dynamics of crystallization I: Theory. Contributions to Mineralogy and Petrology, 99, 277–291.

——— (1998) On the interpretation of crystal size distributions in magmatic systems. Journal of Petrology, 39, 553–599.

Marsh, B.D. and Higgins, M.D. (2002) Inherited correlation in crystal size distribution: Comment. Geology, 30, 284–285.

Miller, C.D. (1985) Holocene eruptions at the Inyo volcanic chain, California: Implications for possible eruptions in Long Valley Caldera. Geology, 13, 14–17.

Pan, Y. (2001) Inherited correlation in crystal size distribution. Geology, 29, 227–230.

——— (2002) Closure in crystal size distributions (CSD), verification of CSD calculations, and the significance of CSD fans: Comment. American Mineralogist, 97, 1242–1243.

Peterson, T.D. (1996) A refined technique for measuring crystal size distributions in thin section. Contributions to Mineralogy and Petrology, 124, 395–405.

Randolf, A.D. and Larson, M.A. (1971) Theory of particulate processes. Academic Press, New York, 251 pp.

Sahagian, D.L. and Proussevitch, A.A. (1998) 3D particle size distributions from 2D observations: stereology for natural applications. Journal of Volcanology and Geothermal Research, 84, 173–196.

Saltikov, S.A. (1967) The determination of the size distribution of particles in an opaque material from a measurement of the size distribution of their sections. In H. Elias, Ed., Proceedings of the Second International Congress for Stereology, p, 163–173. Springer-Verlag, Berlin.

Schaeben, H., van den Boogaart, K.G., Mock, A., and Breitkreuz, C. (2002) Inherited correlation in crystal size distribution; Comment. Geology, 30, 282–283.

Swanson, S.E., Naney, M.T., Westrich, H.R., and Eichelberger, J.C. (1989) Crystallization history of Obsidian Dome, Inyo Domes, California. Bulletin of Volcanology, 51, 161–176.

Underwood, E.E. (1970) Quantitative stereology. 274 p. Addison-Wesley, Reading, Massachusetts.

Vogel, T.A., Eichelberger, J.C., Younker, L.W., Schuraytz, B.C., Horkowitz, J.P., Stockman, H.W., and Westrich, H. R. (1989) Petrology and emplacement dynamics of intrusive and extrusive rhyolites of Obsidian Dome, Inyo Craters Volcanic Chain, Eastern California. Journal of Geophysical Research, 94, 17,937–17,956.

Wager, L.R. (1961) A note on the origin of ophitic texture in the chilled olivine gabbro of the Skaergaard intrusion. Geological Magazine, 989, 353–366.

Waters, C. and Boudreau, A.E. (1996) A reevaluation of crystal size distributions in chromite cumulates. American Mineralogist, 81, 1452–1459.

Wilhelm, S. and Worner, G. (1996) Crystal size distribution in Jurassic Ferrar flows and sills (Victoria Land, Antarctica): evidence for processes of cooling, nucleation, and crystallization. Contributions to Mineralogy and Petrology, 125, 1–15.

Zieg, M.J. and Marsh, B.D. (2002) Crystal size distributions and scaling laws in the quantification of igneous textures. Journal of Petrology, 43, 85–101.

MANUSCRIPT RECEIVED SEPTEMBER 27, 2002
MANUSCRIPT ACCEPTED APRIL 2, 2003
MANUSCRIPT HANDLED BY MARC HIRSCHMANN